

A statistical method to search for recoiling supermassive black holes in active galactic nuclei

P. Raffai^{1,2*}, Z. Haiman³, and Z. Frei^{1,2}

¹*Institute of Physics, Eötvös University, 1117 Budapest, Hungary*

²*MTA-ELTE EIRSA “Lendület” Astrophysics Research Group, 1117 Budapest, Hungary*

³*Department of Astronomy, Columbia University, New York, NY 10027, USA*

Released 2015 Xxxxx XX

ABSTRACT

We propose an observational test for gravitationally recoiling supermassive black holes (BHs) in active galactic nuclei, based on a correlation between the velocities of BHs relative to their host galaxies, $|\Delta v|$, and their obscuring dust column densities, Σ_{dust} (both measured along the line of sight). We use toy models for the distribution of recoil velocities, BH trajectories, and the geometry of obscuring dust tori in galactic centres, to simulate 2.5×10^5 random observations of recoiling quasars. BHs with recoil velocities comparable to the escape velocity from the galactic centre remain bound to the nucleus, and do not fully settle back to the centre of the torus due to dynamical friction in a typical quasar lifetime. We find that $|\Delta v|$ and Σ_{dust} for these BHs are positively correlated. For obscured ($\Sigma_{\text{dust}} > 0$) and for partially obscured ($0 < \Sigma_{\text{dust}} \lesssim 2.3 \text{ g/m}^2$) quasars with $|\Delta v| \geq 45 \text{ km/s}$, the sample correlation coefficient between $\log_{10}(|\Delta v|)$ and Σ_{dust} is $r_{45} = 0.28 \pm 0.02$ and $r_{45} = 0.13 \pm 0.02$, respectively. Allowing for random $\pm 100 \text{ km/s}$ errors in $|\Delta v|$ unrelated to the recoil dilutes the correlation for the partially obscured quasars to $r_{45} = 0.026 \pm 0.004$ measured between $|\Delta v|$ and Σ_{dust} . A random sample of $\gtrsim 3,500$ obscured quasars with $|\Delta v| \geq 45 \text{ km/s}$ would allow rejection of the no-correlation hypothesis with 3σ significance 95 per cent of the time. Finally, we find that the fraction of obscured quasars, $\mathcal{F}_{\text{obs}}(|\Delta v|)$, decreases with $|\Delta v|$ from $\mathcal{F}_{\text{obs}}(< 10 \text{ km/s}) \gtrsim 0.8$ to $\mathcal{F}_{\text{obs}}(> 10^3 \text{ km/s}) \lesssim 0.4$. This predicted trend can be compared to the observed fraction of type II quasars, and can further test combinations of recoil, trajectory, and dust torus models.

Key words: black hole physics — methods: observational — galaxies: active — galaxies: nuclei.

1 INTRODUCTION

Both theoretical models (Begelman, Blandford & Rees 1980; Volonteri, Haardt & Madau 2003) and observations (e.g. Comerford et al. 2009) suggest that it is common for supermassive black holes (SMBHs) in galactic centres to form binaries that gradually lose their energy through radiating gravitational waves (e.g. Haehnelt 1994; Sesana et al. 2005). Numerical simulations of black hole (BH) binary mergers (see e.g. Healy, Lousto & Zlochower 2014 and references therein) suggest that the merger remnant SMBHs receive a recoil velocity of typically several hundred (and in some spin and mass-ratio configurations up to thousands) of km/s, due to highly anisotropic gravitational-wave emission in the final merger phase. Taking into account the spatial distribution of mass in the galactic centre

region, and corresponding dynamical friction, this means that the SMBH can engage in a damped oscillating motion (Madau & Quataert 2004; Komossa & Merritt 2008; Tanaka & Haiman 2009) with an amplitude comparable to, or exceeding the $\mathcal{O}(10\text{-}100 \text{ pc})$ size of the optically thick dusty molecular torus (‘dust torus’) believed to be surrounding galactic centres (for an overview, see Hönig 2008). For a large recoil, the SMBH can escape from the galactic centre and can remain wandering within the dark matter halo (Guedes et al. 2009, 2011). As accreting material can stay gravitationally bound to the moving SMBH, and thus the SMBH can remain active for $10^7 - 10^8 \text{ yr}$ after the merger event (e.g. Loeb 2007), kinematic and spatial signatures of the recoil could be found in the spectra of quasars (QSOs; see e.g. Bonning, Shields & Salviander 2007; Blecha et al. 2011; Komossa 2012; Blecha et al. 2015). These signatures could confirm the gravitational recoil of merger remnant SMBHs, and could probe the SMBH binary parameters, recoil tra-

* E-mail: praffai@bolyai.elte.hu (PR);

jectory models, as well as the spatial distribution and composition of matter in the galactic centre region.

In this paper, we propose that in the presence of dust tori obscuring galactic nuclei, the gravitational recoil of active merger remnant SMBHs should introduce a correlation between dust column mass densities along the line of sight (Σ_{dust}) and magnitudes of line-of-sight peculiar velocities of SMBHs relative to their host galaxies ($|\Delta v|$). Proxies to estimate both of these quantities can be measured from observable features of QSO spectra (Bonning, Shields & Salviander 2007; Ledoux et al. 2015). As pointed out earlier by Komossa & Merritt (2008), recoiling BHs can spend a significant fraction of their time off-nucleus, possibly reducing the fraction of fully obscured ('type II') QSOs; we also follow up on this suggestion.

Using a selected combination of models of gravitational recoil, SMBH trajectories, and obscuring dust tori, we demonstrate the feasibility of detecting $\Sigma_{\text{dust}}-|\Delta v|$ correlations by simulating a set of 2.5×10^5 random observations of recoiled QSOs with a Monte Carlo method. We characterize the strength of correlation between Σ_{dust} and $|\Delta v|$ for obscured (i.e. $\Sigma_{\text{dust}} > 0$) QSOs in two different $|\Delta v|$ intervals, and estimate the number of obscured QSOs that could be used to reject the hypothesis of no correlation between Σ_{dust} and $|\Delta v|$ with 3σ significance. As the strength of the correlation between Σ_{dust} and $|\Delta v|$, as well as the underlying $\Sigma_{\text{dust}}(|\Delta v|)$ relation depends on the presumed combination of models, observational studies on QSO spectra could provide an opportunity for testing chosen combinations of these models. We also calculate the fraction of QSOs obscured by their dust tori, $\mathcal{F}_{\text{obs}}(|\Delta v|)$, which, compared to the observed fraction of type II (i.e. obscured) QSOs could provide an independent test for a chosen combination of recoil, SMBH trajectory, and dust tori models. We propose to use the SDSS-DR10 Quasar Catalog (Pâris et al. 2014) to perform these tests in the near future, and will report on this observational search in a separate publication.

The paper is organized as follows. In § 2, we describe the gravitational recoil and SMBH trajectory models we used in our Monte Carlo simulations. In § 3, we describe our implementation of a smooth dust torus model. We present our results in § 4 and discuss some issues that will be relevant for an observational search for the proposed correlations in § 5. Finally, we offer our conclusions and summarize the implications of this work in § 6.

2 BH DYNAMICS

Anisotropic emission of gravitational waves emitted by coalescing SMBHs carry away linear momentum, resulting in a recoil of the merger remnant SMBH in the opposite direction. Numerical simulations of this process have been carried out for merging SMBHs with equal and unequal masses, zero and non-zero spins aligned or counter-aligned with the orbital angular momentum, and with spins pointing in random directions with equal probability (see e.g. Healy, Lousto & Zlochower 2014 and references therein).

To keep our Monte Carlo simulation as general and realistic, but at the same time, as computationally cheap as possible, following Tanaka & Haiman (2009), we adopted the analytical formulae given in equation (4) of Baker et al.

(2008) to construct the distribution of recoil velocity magnitudes, v_{recoil} (note that Baker et al. 2008 gives results very similar to more recent, slightly modified formulae in Lousto et al. 2012 and Healy, Lousto & Zlochower 2014).

The direction of the recoil velocity depends on the orientation of the spin and orbital angular momentum vectors. It is plausible that prior to merger, the BHs accrete a significant amount of gas coherently from a circumbinary accretion disc, whose inner regions are aligned with the binary's orbital plane (e.g. Ivanov, Papaloizou & Polnarev (1999)). One then expects that the spin angular momentum vectors at the time of the merger may be aligned with the orbital angular momentum of the binary (Bogdanović, Reynolds & Miller 2007; although there could still be significant misalignment at merger for fast-spinning and unequal-mass binaries; Gerosa et al. 2015). Thus, the kick direction may not be random, and may lie preferentially in the plane of the circumbinary disc (and also in the binary orbital plane). However, we emphasize that here we are interested only in the kick direction relative to the orientation of the larger scale nuclear torus. It is much less clear whether the binary orbital plane and/or accretion disc is aligned with the symmetry plane of this torus. This depends on the transfer of angular momentum between large (100 pc) and small (sub-parsec) scales, which is sensitive to turbulence, star formation, and feedback processes (Dubois et al. 2014). Observationally, parsec-scale maser discs (which could be taken as proxies for the accretion discs that determine the kick direction) appear to be oriented randomly with respect to the plane of their host galaxies (Kormendy & Ho 2013). We therefore simply assume that the kick direction is random, i.e. not aligned with the symmetry plane of the torus. Thus, we chose directions of recoil velocities randomly from a uniform distribution covering a whole sphere.

Using the fitting formulae of Baker et al. (2008), we calculated v_{recoil} for a given pair of masses ($m_{1,2}$) and dimensionless spin vectors of the merging SMBHs ($\vec{\alpha}_{1,2} \equiv c\vec{S}_{1,2}/Gm_{1,2}^2$, where $\vec{S}_{1,2}$ are the spins of the SMBHs, c is speed of light, and G is Newton's constant). Observations of active galactic nuclei (AGNs) indicate that a significant number of SMBHs have $|\vec{\alpha}_{1,2}| > 0.9$, although a second population of SMBHs with $0.4 < |\vec{\alpha}_{1,2}| < 0.8$ was found for $m_{1,2} > 4 \times 10^7 M_{\odot}$ SMBHs (see Reynolds 2013). In our simulations, for simplicity, we first assigned each merging SMBH to one of the two $|\vec{\alpha}_{1,2}|$ populations with equal probability, and then drew a random $|\vec{\alpha}_{1,2}|$ value from the corresponding (i.e. $|\vec{\alpha}_{1,2}| \in [0.9, 1]$ or $|\vec{\alpha}_{1,2}| \in [0.4, 0.8]$) interval. The directions of both spin vectors were chosen independently from a uniform distribution covering a whole sphere.

We randomized pairs of masses independently from the SMBH mass function given in Aller & Richstone (2002), downscaled both mass values by a factor of 2, and used them as values for m_1 and m_2 . The fact that we chose the mass of the merger remnant as $M = m_1 + m_2$ means that in our Monte Carlo simulations M values are under-represented at the lowest ($\sim 10^5 M_{\odot}$) and at the highest ($\sim 10^8 M_{\odot}$) values, and overrepresented at values in between, compared to the SMBH mass function given in Aller & Richstone (2002). Fig. 1 shows the histograms M and v_{recoil} values we obtained by randomizing 2.5×10^5 pairs of merging SMBHs.

Using the above set of v_{recoil} 's with uniformly distributed random directions, we simulated the resulting

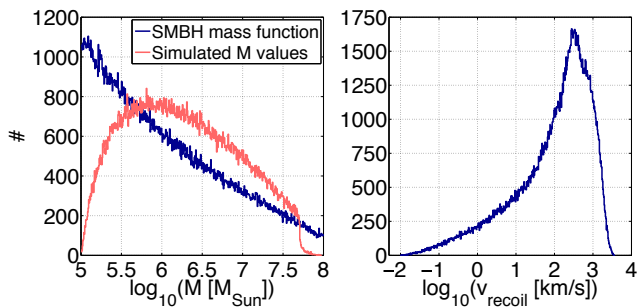


Figure 1. Left: histogram of 2.5×10^5 simulated merger remnant SMBH masses $M = m_1 + m_2$ (red curves), where the values of $2m_1$ and $2m_2$ were randomized from the SMBH mass function given in Aller & Richstone (2002) and represented by dark blue curves. As a result of the randomization process, M values are under-represented at the lowest ($\sim 10^5 M_\odot$) and at the highest ($\sim 10^8 M_\odot$) values, and overrepresented at values in between, compared to the SMBH mass function. Right: histogram of the corresponding recoil velocity magnitudes, v_{recoil} , of the merger remnant SMBHs, obtained using the framework presented in Baker et al. (2008), and assuming that merging SMBHs have dimensionless spin magnitudes, $|\vec{\alpha}_{1,2}|$, from two distinct populations (i.e. $|\vec{\alpha}_{1,2}| \in [0.9, 1]$ and $|\vec{\alpha}_{1,2}| \in [0.4, 0.8]$; see Reynolds 2013) with equal probability, that $|\vec{\alpha}_{1,2}|$ values are uniformly distributed within each of the two $|\vec{\alpha}_{1,2}|$ intervals, and that $\vec{\alpha}_{1,2}$ have uniformly distributed random directions.

SMBH trajectories based on the model presented in Madau & Quataert (2004). The initial position of the SMBH and the origin of our coordinate system were chosen to coincide with the galactic centre. This model assumes that the SMBH is embedded in a spherical stellar bulge, and is decelerated by dynamical friction. The one-dimensional velocity dispersion of stars in the bulge were calculated using the empirical M - σ relation (Tremaine et al. 2002) as $\sigma_{1D} = (1/\sqrt{3}) \times (M/1.3 \times 10^8 M_\odot)^{1/4} 200$ km/s. According to observations by Barth, Greene & Ho (2005) and Greene & Ho (2006), this relation extends to active SMBHs with masses as low as $M \sim 10^5 M_\odot$. We simulated the trajectories with a $\Delta t = 10^3$ yr time resolution up to a randomly picked final time between $T \in [\Delta t, 3 \times 10^4 \Delta t]$. The maximum duration of $T_{\text{max}} \equiv 3 \times 10^4 \Delta t = 3 \times 10^7$ yr was chosen to be comparable with the maximum known duration of QSO activity (see Martini 2004 for a review). The simulation was terminated before T if the orbit of the SMBH has decayed and the SMBH settled back at the galactic centre (i.e. if the radial distance, d , and radial velocity, v_r , of the SMBH converged to $d < 10^{-2}$ pc and $v_r < 10^{-2}$ km/s, respectively). The position, velocity, and Δv of the SMBH in its final state were calculated and stored, as if they were results of a QSO observation made at a random time during the QSO activity after the recoil. Histograms of d and v_r values obtained for the 2.5×10^5 QSOs are shown in Fig. 2. Note that we assumed that recoiled SMBHs remain active along their entire trajectory, and also that they are active at the time the mock observation is made.

Guedes et al. (2009) followed the motions of merger remnant SMBHs with fixed masses in various configurations of dark matter haloes using numerical simulations. They concluded that due to the asymmetric and inhomogeneous mass distribution in the halo, the SMBH trajectories suffer

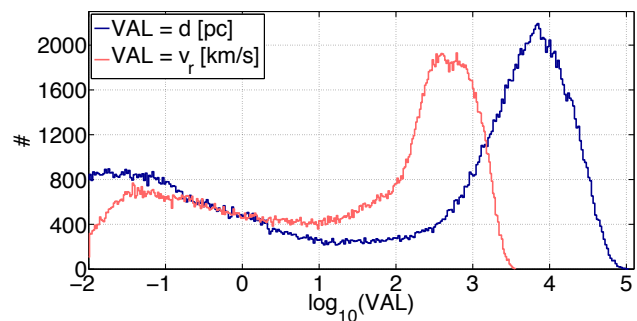


Figure 2. Histogram of distance d (in pc; blue curve), and radial velocity magnitude, v_r (in km/s; red curve), of the 2.5×10^5 SMBHs, both measured from the galactic centre at the randomly picked time of a mock observation. Both histograms show bimodality. The peaks at lower d and v_r values ($\log_{10}(\text{VAL}) < -1$) correspond to SMBHs that underwent at least a half period of oscillation and thus suffered a strong orbital decay due to dynamical friction in the galactic centre. The peaks at high ($\log_{10}(\text{VAL}) > 2$) d and v_r values correspond to SMBHs whose initial recoil velocity was high enough to make them gravitationally unbound and escape from the galactic centre region.

large deviations from the Madau & Quataert (2004) trajectories. SMBHs might not even return to the galactic centre, after the SMBHs reach the first turning point in their oscillating motion. To check how much this could affect the results of our Monte Carlo simulations, we simulated an independent set of 10^5 QSOs, and examined the fraction of SMBHs that reach the first turning point before the mock observation is made. We found that for the entire QSO sample, this fraction is $\simeq 31$ per cent, while it is reduced to $\simeq 11$ and $\simeq 4$ per cent for QSOs with $|\Delta v| \geq 5$ km/s and $|\Delta v| \geq 45$ km/s, respectively. The reason for the full population having a higher fraction is that once the SMBHs make their first U-turn, their orbits decay rapidly due to dynamical friction. As a result, many of these end up with $|\Delta v| < 5$ km/s and $|\Delta v| < 45$ km/s at the mock observation time (as shown in Fig. 2). As we will show in § 4 below, only QSOs with $|\Delta v| \geq 5$ km/s show a $\Sigma_{\text{dust}} - |\Delta v|$ correlation. Furthermore, below we propose to study only the subset of QSOs with $|\Delta v| \geq 45$ km/s, due to the limitations imposed by inevitable random velocity errors. We conclude that in this sub-sample of QSOs, the effects of asphericity and inhomogeneities will reduce the predicted correlations only by ≈ 4 per cent, and we ignore this complication in the rest of this paper.

A similar deviation from a purely radial trajectory may arise on much smaller scales, inside the spherical nuclear star cluster (stellar core) enshrouding the galactic centre. As shown by Gualandris & Merritt (2008), when the SMBH mass is not negligible compared to the mass of the stellar core, the SMBH and the stellar core exhibit oscillations about their common centre of mass. As a result, the SMBH is not exposed to the largest dynamical friction near the geometric centre of the core, and it may take up to ~ 10 times longer for the oscillations to be damped. Here, we neglect this effect, leaving its evaluation to future work. However, we note that it would likely result in a larger fraction of SMBHs remaining displaced from the nucleus, and possibly a larger fraction of QSOs exhibiting the correlations we propose.

3 TORUS MODEL

According to the unified scheme of AGNs, galactic nuclei are obscured by optically and geometrically thick dusty molecular tori, with the amount of obscuration depending on the viewing angle (Antonucci 1993). Even though dust typically only constitutes ~ 1 per cent of the mass of the tori (while the rest of the mass is in gas, mostly in molecular hydrogen form), dust is the main component responsible for the obscuration and reddening of QSOs, and thus, most torus models focus on the dust distribution in the tori (i.e. on ‘dust tori’).

Torus models developed to reproduce the observed spectral energy distributions of AGNs can be divided into two categories: smooth versus clumpy models (for an overview, see e.g. Hönig 2008). We implemented a hydrostatic model of smooth dust tori presented by Schartmann et al. (2005). This model has the advantages of simplicity, using physically reasonable assumptions about torus formation, and providing good fits to the mid-infrared spectral energy distributions of AGNs with relatively few free parameters. The dust torus is assumed to form from gas released through stellar winds and ejection of planetary nebulae in the nuclear star cluster. Even though the ejecta of individual stars should produce a cloudy structure of the torus, no instruments so far has been able to resolve single clouds of the dust distribution, and Schartmann et al. (2005) conclude that these clouds should be small. For simplicity, they treat the torus as a continuous medium characterized by the density distribution ρ_d (see their equation 8). The effective potential created by the central SMBH and the angular momentum distribution in the stellar core makes ρ_d axisymmetric around the galactic centre.

To cover the range of masses M_* of the nuclear star clusters in the examples in Schartmann et al. (2005) and the observations presented in Leigh, Böker & Knigge (2012), we chose $M_* = 10^{5+\beta} M_\odot$, where β was drawn from a uniform distribution in the range $\beta \in [0, 4]$. We set the mass of the dust enclosed in the torus to $M_{\text{dust}} = (5.79 \times 10^5 M_\odot) \times [M_*/(2 \times 10^9 M_\odot)]$ in order to reproduce parameter values of the example torus given in table 1 in Schartmann et al. (2005).

The radius of the stellar core, R_c , was chosen to be

$$R_c = 2 \times 10^{(a \log_{10}[M_*/M_\odot] - b)} \text{ pc}, \quad (1)$$

where the dimensionless constants $a = 0.3042$ and $b = 1.2679$ were obtained by fitting the half-light core radii, $r_{\text{eff}} = 0.5 R_c$, for late- and early-type galaxies in Figure 13 in Georgiev & Böker (2014). Note that we assumed a constant stellar mass-to-light ratio, M_*/L_V , where L_V is the total luminosity of the nuclear star cluster in the V band.

The radius R_T of the torus was chosen such that the sizes of the torus and of the nuclear star cluster are comparable, with $R_T = 5$ pc for $M_* = 2 \times 10^9 M_\odot$ (see table 1 in Schartmann et al. 2005):

$$R_T = 3.56 \times 10^{-2} R_c + 2.33 \text{ pc}. \quad (2)$$

For all other parameters in our torus simulations, we followed the methods in Schartmann et al. (2005). Specifically, we set the outer radius of the torus $R_{\text{out}} = 3R_c$, the exponent of the angular momentum distribution in the stellar core $\gamma = -0.5$, and the turbulent velocity of the clouds building up the torus $v_t \approx \sigma_*$, where we used equation (9) in

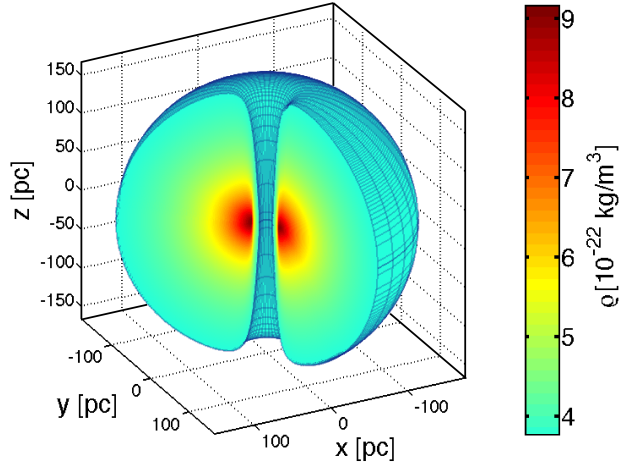


Figure 3. An example for the adopted geometry and interior density structure along a cross-section of a torus surrounding an AGN, based on Schartmann et al. (2005). The mass of the nuclear star cluster containing the torus and producing its dust content was chosen to be $M_* = 10^9 M_\odot$, while the mass of the central SMBH was set to $M = 10^6 M_\odot$.

Schartmann et al. (2005) to calculate the velocity dispersion of the stars in the nuclear star cluster, σ_* .

The density distribution of a torus in this model is fully determined by two parameters: the mass of the nuclear star cluster, M_* , and the mass of the central SMBH, M . Using the random values of M_* and M , for each torus we calculated $\hat{\rho}_d(R, z) \equiv \rho_d(R, z)/\rho_d^0$ (see Eq. 8 in Schartmann et al. 2005) in a $R_{\text{out}} \times R_{\text{out}}$ rectangular cross-section along the $R - z$ plane with a linear resolution of $R_{\text{out}}/200$, set $\hat{\rho}_d(R, z) = 0$ wherever $\hat{\rho}_d(R, z) < \hat{\rho}_d(R_{\text{out}}, 0)$, and calculated ρ_d^0 such that the total mass of the torus with the resulting $\rho_d(R, z)$ equals M_{dust} . In our simulation, only the dust column mass density, Σ_{dust} , was recorded as the final output, which was calculated by numerically integrating $\rho_d(R, z)$ along the line of sight from each SMBH position to the observer for a randomly oriented torus.

For illustration, Fig. 3 shows a visualization of the geometry and interior density structure (ρ_d) along a cross-section of a torus with $M_* = 10^9 M_\odot$ and $M = 10^6 M_\odot$. Additionally, in Fig. 4, we show the histogram of the outer radii, R_{out} , of the 2×10^5 dust tori. This shows that the outer radii follow a $\propto 1/R_{\text{out}}$ distribution, ranging from $R_{\text{out, min}} \simeq 10$ pc to $R_{\text{out, max}} \simeq 180$ pc.

4 RESULTS

We are now ready to present the results of the Monte Carlo simulation of 2.5×10^5 random observations of recoiling QSOs. In Fig. 5, we show the histogram of dust column mass densities (Σ_{dust}) obtained by integrating the mass density of the randomly oriented dust tori along the line-of-sight to the recoiling SMBH (dark blue curve). For reference, we also show a Σ_{dust} histogram for a second set of simulations of 2.5×10^5 QSOs with recoil velocities set to $v_{\text{recoil}} = 0$ (light red curve). We have found that the total number of unobscured QSOs (i.e. with $\Sigma_{\text{dust}} = 0$) is $\sim 152,700$ ($\simeq 61$ per cent) and $\sim 44,200$ ($\simeq 18$ per cent) for the $v_{\text{recoil}} > 0$

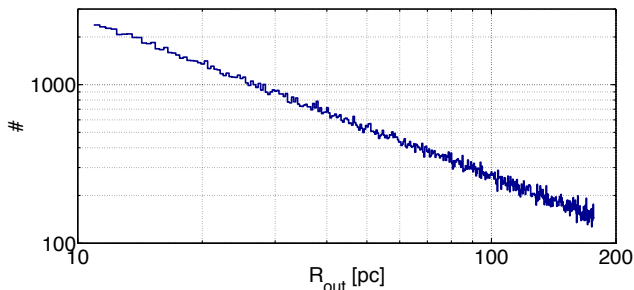


Figure 4. Histogram of outer radii, R_{out} , of the 2×10^5 simulated dust tori. R_{out} values follow a $\propto 1/R_{\text{out}}$ distribution, ranging from $R_{\text{out,min}} \simeq 10$ pc to $R_{\text{out,max}} \simeq 180$ pc.

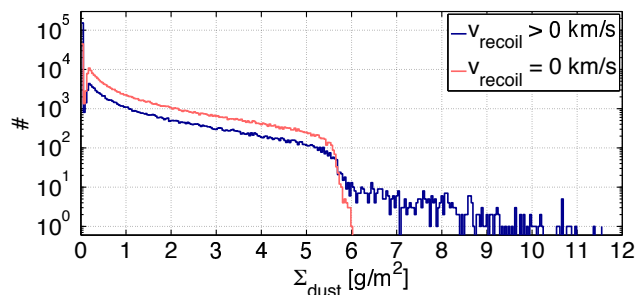


Figure 5. Histogram of dust column mass densities (Σ_{dust}) for 2.5×10^5 random observations of QSOs, obtained by integrating the mass density of the randomly oriented dust tori along the line of sight to the recoiling, off-centre SMBHs (dark blue curve). For reference, we show the same histogram for a similar sample of QSO without any recoil ($v_{\text{recoil}} = 0$; light red curve). The recoiling QSOs are much more likely to be seen completely unobscured (there are ~ 152700 ($\simeq 61$ per cent) and ~ 44200 ($\simeq 18$ per cent) QSOs with $\Sigma_{\text{dust}} = 0$ in the samples with and without recoil, respectively). The recoiling QSOs also show a tail of high Σ_{dust} values up to twice the maximum value for non-recoiling QSOs, as expected (see text).

and $v_{\text{recoil}} = 0$ samples, respectively. QSOs in the $v_{\text{recoil}} = 0$ sample do not have Σ_{dust} values above $\Sigma_{\text{dust}} \simeq 6$ g/m² because such QSOs are never obscured by more than a half cross-section of their dust torus, and a half cross-section of any dust tori in the Schartmann et al. (2005) model have a maximum possible dust column density of $\Sigma_{\text{torus}} \simeq 6$ g/m². Recoiling QSOs ($v_{\text{recoil}} > 0$ km/s) can obtain up to twice higher values of Σ_{dust} (i.e. up to $\Sigma_{\text{dust}} \simeq 12$ g/m²), which corresponds to the maximal obscuration of a QSO located in the ‘equatorial plane’, behind the dust torus (and for the geometrically largest tori). This configuration is rare, with only 409 ($\simeq 0.2$ per cent) QSOs in the $v_{\text{recoil}} > 0$ sample having $\Sigma_{\text{dust}} > 6$ g/m².

Fig. 6 shows Σ_{dust} versus $|\Delta v|$ for the 2.5×10^5 recoiling QSOs. We have calculated the sample correlation coefficient, r , between Σ_{dust} and $\log_{10}(|\Delta v|)$, defined by

$$r \equiv \frac{\langle \Sigma_{\text{dust}} \log_{10}(|\Delta v|) \rangle - \langle \Sigma_{\text{dust}} \rangle \langle \log_{10}(|\Delta v|) \rangle}{\sqrt{\langle \Sigma_{\text{dust}}^2 \rangle - \langle \Sigma_{\text{dust}} \rangle^2} \sqrt{\langle \log_{10}(|\Delta v|)^2 \rangle - \langle \log_{10}(|\Delta v|) \rangle^2}}, \quad (3)$$

restricted to various ranges of $|\Delta v|_{\text{min}} \leq |\Delta v| \leq |\Delta v|_{\text{max}}$. Here $\langle \dots \rangle$ refers to averaging over the sample of 2.5×10^5 QSOs, or its various subsets.

Fig. 7 shows r as a function of $|\Delta v|_{\text{min}}$ (left-hand panels) and $|\Delta v|_{\text{max}}$ (right-hand panels) for sub-samples of obscured QSOs with $|\Delta v| \geq |\Delta v|_{\text{min}}$ and $|\Delta v| < |\Delta v|_{\text{max}}$, respectively. As can be seen in the figure, obscured QSOs with $|\Delta v| < 5$ km/s show no correlation between their Σ_{dust} and $|\Delta v|$ values ($r_{<5} \simeq 0$, and the corresponding p -value for the hypothesis of no correlation is $p \simeq 0.95$), while QSOs with $|\Delta v| \geq 5$ km/s show a significant correlation, with $r_5 = 0.22 \pm 0.01$ and $p \simeq 0$. The correlation coefficient increases with $|\Delta v|_{\text{min}}$ until it reaches its maximum at $|\Delta v|_{\text{min}} = 45$ km/s with $r_{45} = 0.28 \pm 0.02$.

Allowing $|\Delta v|_{\text{min}}$ and $|\Delta v|_{\text{max}}$ to vary simultaneously does not change the result that r is the highest for the 3,824 obscured QSOs with $|\Delta v| \geq 45$ km/s. Depending on the signal to noise, the measurement error on $|\Delta v|$ of individual QSOs is a few tens of km/s (for example from spectral line fitting, or by using the centroids of individual broad lines; see e.g., Ju et al. 2013; Shen et al. 2013). We therefore restrict our further investigations to the 3824 obscured QSOs with $|\Delta v| \geq 45$ km/s. For this subset, we have found the approximate relation $\Sigma_{\text{dust}} (\log_{10}\{|\Delta v|\}) = (1.7 \pm 0.1) \text{ g/m}^2 \times (\log_{10}\{|\Delta v|/[1 \text{ km/s}]\}) - (1.3 \pm 0.2) \text{ g/m}^2$, although of course this relation depends strongly on the underlying set of models. We also note that in addition to the random measurement errors on $|\Delta v|$, broad line centroids can shift by $\mathcal{O}(100 \text{ km/s})$ between pairs of observations only weeks apart, for physical reasons unrelated to recoil (Ju et al. 2013; Shen et al. 2013). These shifts, as well as the measurement errors, are not expected to correlate with Σ_{dust} . However, they introduce random errors on the $\Sigma_{\text{dust}} (\log_{10}(|\Delta v|))$ relation, and can therefore increase the number of QSOs required to detect the underlying $\Sigma_{\text{dust}} - \log_{10}(|\Delta v|)$ correlation (see discussion below).

We next estimate the minimum number of QSOs, N_{min} , required for a significant detection of the correlation. To do this, for each trial $N \in [10, 350]$ QSOs, we (i) generated 1000 independent random samples of N QSOs, selected from among the 3824 obscured QSOs recoiling with $|\Delta v| \geq 45$ km/s, (ii) computed the p -value of the hypothesis of no correlation between Σ_{dust} and $|\Delta v|$ for each of these 1000 samples, and (iii) measured the fraction of samples for which $p < 3 \times 10^{-3}$ (corresponding to the rejection of the no-correlation hypothesis at 3σ confidence). This fraction, $F_{3\sigma}$, is shown in Fig. 8 (blue crosses, right-hand panel), together with the average $\langle r \rangle$ over the 1000 random samples, as a function of N (blue crosses, left-hand panel).

As a test of these statistics, we have repeated the calculations of both $\langle r \rangle$ and $F_{3\sigma}$ for two additional sequences of 1000 random samples of $N \in [10, 350]$ QSOs. In the first set, we began with recoiling QSOs with $|\Delta v| < 5$ km/s; the results are shown by the red empty circles in Fig. 8). In the second set, we computed random Σ_{dust} values for stationary SMBHs ($v_{\text{recoil}} = 0$), and associated a $|\Delta v|$ with each case, drawn randomly from the $|\Delta v|$ distribution for the recoiling ($v_{\text{recoil}} > 0$) SMBHs. The results for these ‘scrambled’ data” are shown in Fig. 8 by the filled green circles.

As can be seen in Fig. 8, neither the $|\Delta v| < 5$ km/s, nor the ‘scrambled data’ sets show correlations, i.e. $\langle r \rangle \simeq 0$ and $F_{3\sigma} \simeq 0$ for all N . On the other hand, for obscured QSOs with $|\Delta v| \geq 45$ km/s, we find $\langle r \rangle \simeq 0.28$ for all N , and $F_{3\sigma}$ increases monotonically with N from $F_{3\sigma} \simeq 0$ to $F_{3\sigma} \simeq 1$ within the interval $N \in [10, 350]$. We conclude

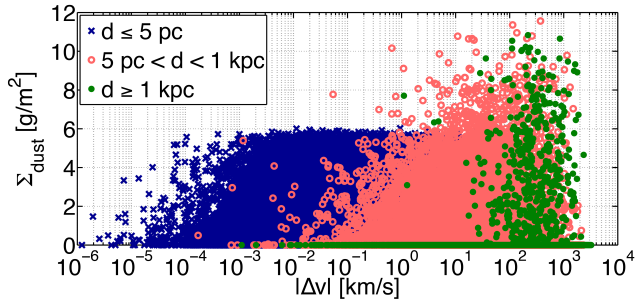


Figure 6. The line-of-sight dust column density, Σ_{dust} , versus the (absolute value) of line-of-sight velocity offset $|\Delta v|$ relative to the host galaxy, for each of the 2.5×10^5 recoiling QSO. For completeness, we show the entire range of velocities we simulated, down to unmeasurably low values. To illustrate how far each recoiling QSO has travelled from the galactic centre by the time of the mock observation, we sorted the data into three groups, based on their radial offset d from the galactic centre: QSOs with the smallest offset ($d \leq 5$ pc; blue crosses), QSOs with offsets within roughly an order of magnitude of the size of their parent torus ($5 \text{ pc} < d < 1 \text{ kpc}$; red circles), and the most distant QSOs ($d \geq 1 \text{ kpc}$; green full circles). The distribution of points shows three distinct Σ_{dust} values: $\Sigma_{\text{dust}} = 0$ (corresponding to the ejected QSOs with the largest offsets, viewed in an unobscured direction), $\Sigma_{\text{dust}} \simeq 6 \text{ g/m}^2$ (the maximum possible obscuration in the Schartmann et al. (2005) model by half of the torus, for QSOs whose orbits have fully decayed back to the centre by dynamical friction and are viewed along the equator), and at $\Sigma_{\text{dust}} \simeq 12 \text{ g/m}^2$ (the maximum possible obscuration, for QSOs located behind the full torus).

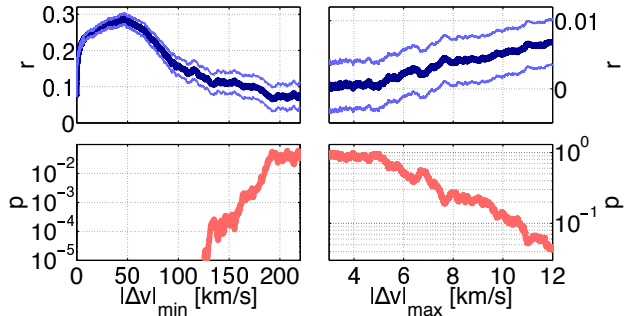


Figure 7. Sample correlation coefficient r between Σ_{dust} and $\log_{10}(|\Delta v|)$, with its 1σ uncertainty (upper panels, blue curves), and the corresponding p values for the hypothesis of no correlation (lower panels, red curves). The left-hand (right-hand) panels show both r and p as a function of $|\Delta v|_{\text{min}}$ ($|\Delta v|_{\text{max}}$), for sub-samples of obscured QSOs with $|\Delta v| \geq |\Delta v|_{\text{min}}$ ($|\Delta v| < |\Delta v|_{\text{max}}$). QSOs with $|\Delta v| \gtrsim 5 \text{ km/s}$ show a positive correlation, with r as high as $r = 0.28 \pm 0.02$ for $|\Delta v|_{\text{min}} \approx 45 \text{ km/s}$.

that the hypothesis of no correlation between Σ_{dust} and $\log_{10}(|\Delta v|)$ could be rejected with a 3σ significance 95 per cent of the time by observing a random sample of ~ 260 obscured QSOs with $|\Delta v| \geq 45 \text{ km/s}$. Note that in our simulations, 3824 QSOs ($\simeq 1.5$ per cent) were obscured having $|\Delta v| \geq 45 \text{ km/s}$, thus gathering a sample of ~ 260 such QSOs may require observing as many as ~ 17000 recoiling QSOs (and a larger number of QSOs in general, accounting

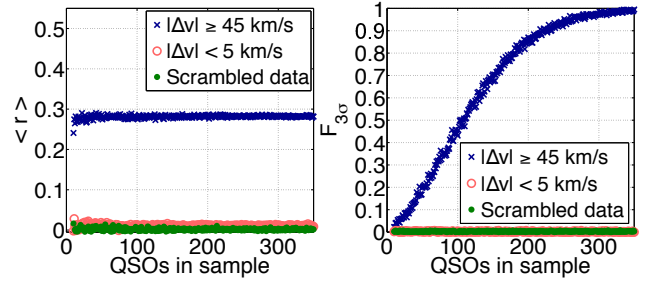


Figure 8. Left-hand panel: the expectation value ($\langle r \rangle$) of the correlation coefficient between Σ_{dust} and $\log_{10}(|\Delta v|)$, computed in 1000 random samples of N QSOs. The results are shown as a function of N in the range $N \in [10, 350]$ for three different QSO data sets: obscured QSOs with $|\Delta v| \geq 45 \text{ km/s}$ (blue crosses), obscured QSOs with $|\Delta v| < 5 \text{ km/s}$ (red circles), and QSOs without recoil, but with $|\Delta v|$ values assigned randomly from the $|\Delta v|$ distribution for recoiling SMBHs (‘scrambled data’; filled green circles). While $\langle r \rangle \simeq 0$ for all N in the last two data sets, the first data set shows a stable correlation with $\langle r \rangle \simeq 0.28$ for all N . Right-hand panel: the fraction $F_{3\sigma}$ of the 1,000 random samples in which the ‘no correlation’ null hypothesis can be rejected at $\geq 3\sigma$ significance. While $F_{3\sigma} \simeq 0$ for the $|\Delta v| < 5 \text{ km/s}$ and ‘scrambled’ data sets, it increases monotonically with N from $F_{3\sigma} \simeq 0$ to 1 for the $|\Delta v| \geq 45 \text{ km/s}$ data set, rising above $F_{3\sigma} \geq 0.95$ for $N \geq 260$.

for the fact that not all QSOs experienced a recoil in the past).

To examine the impact of the sign of the line-of-sight velocity offset, in Fig. 9 we show Σ_{dust} versus $|\Delta v|$ in the subsample of 17157 obscured QSOs with $|\Delta v| \geq 5 \text{ km/s}$, and indicate whether they are moving away from ($\Delta v > 0$, shown as blue crosses) or towards ($\Delta v < 0$, shown as red full circles) the observer. First, we note that receding QSOs are slightly more common, with an excess of 1405 and 1162 in the $|\Delta v| \geq 5 \text{ km/s}$, and $|\Delta v| \geq 45 \text{ km/s}$ samples, respectively, over the approaching cases. As Fig. 9 shows, Σ_{dust} values of the receding QSOs also tend to be higher, especially when the velocity offset is large ($|\Delta v| \gtrsim 100 \text{ km/s}$). This is because receding QSOs are more likely to be found behind, rather than in front of the tori. In order for a SMBH to be approaching with a large line-of-sight velocity while being located behind the torus, it would have had to reach its first U-turn. As mentioned above, the majority of SMBHs with large recoil velocities do not make their first U-turn within a QSO lifetime (or within our mock observation times).

In Fig. 10, we compare the numerically constructed probability density functions of various parameter distributions of QSOs within the whole sample, and within the subsample of obscured QSOs with $|\Delta v| \geq 45 \text{ km/s}$. Based on the comparison, we conclude that AGNs where the central SMBH has a mass around $M \simeq (0.5 - 3) \times 10^6 M_{\odot}$, a positional offset from the centre of the host galaxy between $d_{\text{offset}} \simeq 10^{-1} - 10^2 \text{ pc}$, and having a nuclear star cluster with mass $M_* \gtrsim 10^7 M_{\odot}$, have the highest probability of being in the subset of obscured QSOs with $|\Delta v| \geq 45 \text{ km/s}$. The fact that high-mass nuclear star clusters are over-represented in the subset of QSOs showing $\Sigma_{\text{dust}} - |\Delta v|$ correlation (see the upper-right panel in Fig. 10) suggests that such QSOs are more likely to be found in active galaxies with higher masses. We attribute this to the fact that in more massive galaxies,

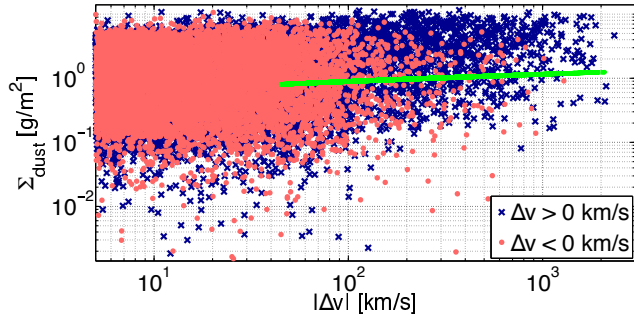


Figure 9. Σ_{dust} versus $|\Delta v|$ for the 17157 obscured QSOs with $|\Delta v| \geq 5$ km/s. Receding (i.e. $\Delta v > 0$) QSOs are shown by blue crosses, while approaching QSOs (i.e. $\Delta v < 0$) are shown by red filled circles. We also show the $\Sigma_{\text{dust}}(\log_{10}(|\Delta v|)) = (1.7 \pm 0.1) \text{ g/m}^2 \times (\log_{10}(|\Delta v|/[1 \text{ km/s}])) - (1.3 \pm 0.2) \text{ g/m}^2$ curve (green solid line) we obtained by fitting Σ_{dust} versus $\log_{10}(|\Delta v|)$ values for obscured QSOs with $|\Delta v| \geq 45$ km/s. Receding SMBHs are slightly more common among the obscured ($\Sigma_{\text{dust}} > 0$) QSOs, their velocity offsets extend to higher values, and they tend to be more heavily obscured (larger Σ_{dust}), especially at large velocity offsets ($\Delta v \gtrsim 100$ km/s). See text for the origin of these differences.

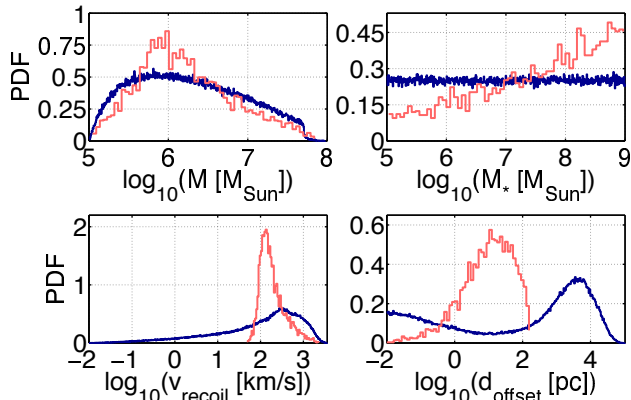


Figure 10. The probability distribution functions of different parameters of the QSOs within the entire sample (blue curves), and within the subsample of obscured QSOs with significant correlations (i.e. with $|\Delta v| \geq 45$ km/s; red curves). The four different panels, clockwise from top left, show the SMBH masses (M), the masses of the nuclear star clusters (M_*), recoil velocities (v_{recoil}), and the offsets of QSOs from the centres of their host galaxies (d_{offset}). The difference between the red and blue curves reveal that QSOs with $M \simeq (0.5 - 3) \times 10^6 M_{\odot}$, $M_* \gtrsim 10^7 M_{\odot}$, $v_{\text{recoil}} \simeq 100$ km/s, and $d_{\text{offset}} \simeq 10^{-1} - 10^2$ pc are the most over-represented in the sample showing strong correlations between Σ_{dust} and $|\Delta v|$.

the recoiling BHs spend longer times at off-centre distances comparable to the size of the obscuring torus. This host-size dependence of the proposed correlation is another potential testable prediction of our toy model.

Finally, we have studied the fraction of obscured QSOs within the whole sample of QSOs, $\mathcal{F}_{\text{obs}}(|\Delta v|)$. We have found that this fraction decreases monotonically with $|\Delta v|$ from $\mathcal{F}_{\text{obs}}(< 10 \text{ km/s}) \gtrsim 0.8$ to $\mathcal{F}_{\text{obs}}(> 10^3 \text{ km/s}) \lesssim 0.4$ (see Fig. 11). This result can be compared in the future to the

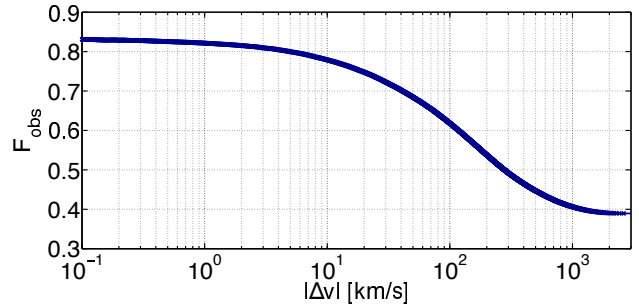


Figure 11. The fraction of obscured ($\Sigma_{\text{dust}} > 0$) sources among the entire sample of 2.5×10^5 QSOs. The trend of $\mathcal{F}_{\text{obs}}(|\Delta v|)$ decreasing with $|\Delta v|$ from $\mathcal{F}_{\text{obs}}(< 10 \text{ km/s}) \gtrsim 0.8$ to $\mathcal{F}_{\text{obs}}(> 10^3 \text{ km/s}) \lesssim 0.4$ could provide an independent test for a chosen combination of recoil, trajectory, and dust tori models, when compared with the observed fraction of obscured (e.g. type II) QSOs in the future.

observed fraction of obscured (e.g. type II) QSOs, which can potentially provide an independent test for a chosen combination of recoil, trajectory, and dust tori models.

5 DISCUSSION

The results in the previous section show that a positive correlation may be present between Σ_{dust} and $|\Delta v|$. We emphasize that this conclusion is based on a specific set of idealized toy models – more realistic models will undoubtedly lead to different predictions. Nevertheless, our results should motivate an observational search; more realistic and flexible models will likely be needed to interpret any correlation discovered in actual data. We plan to present the results from a search in the SDSS DR10 data base in a forthcoming publication.

Here we address two natural caveats: while proxies can be used to estimate both Σ_{dust} and $|\Delta v|$, these estimates will have uncertainties we have so far ignored. Although we have no a priori reason to expect that these uncertainties will be correlated, they will represent noise, which will reduce the statistical significance of any correlation, and thus increase the number of QSOs required for a detection. Furthermore, we have so far assumed that a clean QSO sub-sample with $\Sigma_{\text{dust}} > 0$ and $|\Delta v| \geq 45$ km/s can be constructed. More realistically, observational errors will pollute any such selection (e.g. QSOs with $|\Delta v| \geq 45$ km/s can be missed, and QSOs with $|\Delta v| < 45$ km/s can be mistakenly included).

The line-of-sight velocity offset ($|\Delta v|$) can be estimated using the centroids or peaks of broad lines, relative to those of the narrow lines. The level of obscuration (Σ_{dust}) can be estimated using QSO colours: a larger obscuring column should result in a redder continuum (see e.g. Ledoux et al. (2015) and references therein). An alternative proxy for the obscuring column could be the equivalent width of the broad lines themselves. Although the geometry of the broad line region is not fully understood, type II quasars have weak or no broad emission lines. In the standard unified model of AGN (Antonucci 1993), this is attributed to the obscuration of the high-velocity broad-line region by the dusty torus (note that the continuum is still visible and can therefore not

be spatially colocated with the broad-line emitting region). This implies that the equivalent width of these broad lines must vary with the level of the obscuration.

Here we estimate the impact of having random errors on both $|\Delta v|$ and Σ_{dust} . As mentioned above, we expect $|\Delta v|$, when determined using line centroids, to suffer physical variations of order $\sigma_{\Delta v} \approx 100$ km/s. We therefore repeated our analysis above, except we added a random additional Δv component to the velocity offset of each simulated QSO, drawn from a Gaussian distribution with a standard deviation of $\sigma_{\Delta v}$. For any given $\sigma_{\Delta v}$, we then selected the subset of the 2.5×10^5 QSOs with $\Sigma_{\text{dust}} > 0$ and $|\Delta v| \geq 45$ km/s, as before. Finally, we measured the expectation value of the correlation coefficient $\langle r \rangle$ between $\Sigma_{\text{dust}} > 0$ and $|\Delta v|$ in 1000 randomly drawn sets of N QSOs from this subset, and determined the minimum number N_{min} of QSOs required to infer $r > 0$ with 3σ significance 95 per cent of the time.

The result of this random-velocity-error exercise is shown in Fig. 12 for both $\Sigma_{\text{dust}}-\log_{10}(|\Delta v|)$ and $\Sigma_{\text{dust}}-|\Delta v|$ correlations. The right-hand panel in this figure shows N_{min} as a function of the random error $\sigma_{\Delta v}$. As expected, the number of QSOs required to detect a correlation increase monotonically with $\sigma_{\Delta v}$, rising to $N_{\text{min}} = 3560$ for the $\Sigma_{\text{dust}}-|\Delta v|$ correlation and for $\sigma_{\Delta v} = 100$ km/s; this is more than an order of magnitude increase over the $N_{\text{min}} = 260$ in the idealized case for the $\Sigma_{\text{dust}}-\log_{10}(|\Delta v|)$ correlation without any velocity-offset error. The left-hand panel in Fig. 12 shows the corresponding values of the correlation coefficients; $\langle r \rangle$ decreases monotonically with $\sigma_{\Delta v}$, reaching $\langle r \rangle = 0.091 \pm 0.016$ for the $\Sigma_{\text{dust}}-|\Delta v|$ correlation and for $\sigma_{\Delta v} = 100$ km/s. This is a decrease from the $\langle r \rangle = 0.28 \pm 0.02$ in the idealized case for the $\Sigma_{\text{dust}}-\log_{10}(|\Delta v|)$ correlation by a factor of three. Additionally, we have calculated $\langle r \rangle$ for partially obscured QSOs only (i.e. QSOs with $0 < \Sigma_{\text{dust}} \lesssim 2.3$ g/m²), again assuming $\sigma_{\Delta v} = 100$ km/s, and we have found it to be $\langle r \rangle = 0.026 \pm 0.004$, measured between $|\Delta v|$ and Σ_{dust} .

Similarly to the errors in $|\Delta v|$, we have studied the impact of errors in Σ_{dust} . Here, there are several potential concerns. First, in the presence of uncertainties, a sharp selection $\Sigma_{\text{dust}} > 0$ is unrealistic. Secondly, for large obscuring columns, with Σ_{dust} comparable to the maximum possible column density of a half-torus according to the Schartmann et al. (2005) model (see Fig. 6), $\Sigma_{\text{torus}} \simeq 6$ g/m² (i.e. for configurations corresponding to true type II QSOs), the broad lines may be undetectable, or may have too low S/N for a reliable centroid measurement.¹ We here repeated our fiducial analysis, except that we replaced the selection criterion $\Sigma_{\text{dust}} > 0$ by the range $\Sigma_{\text{min}} < \Sigma_{\text{dust}} < \Sigma_{\text{max}}$. We chose $\Sigma_{\text{min}} = 0.6$ g/m² $\approx 0.1 \times \Sigma_{\text{torus}}$ and $\Sigma_{\text{max}} = 2.3$ g/m² $\approx 0.4 \times \Sigma_{\text{torus}}$. The number of QSOs within this range (and also satisfying $\Delta v \geq 45$ km/s as before) is $N = 1436$, or ~ 0.6 per cent of the full sample of 2.5×10^5 QSOs. With this cut, we find that the correlations remain significant: $\langle r \rangle = 0.098 \pm 0.026$ for the $\Sigma_{\text{dust}}-\log_{10}(|\Delta v|)$ correlation, with a p -value of $p = 2 \times 10^{-4}$.

We also evaluated the impact of random Gaussian errors

¹ Note that the broad lines and the optical continuum are thought to arise from different spatial locations, and can suffer different levels of obscuration; we ignore this complication here.

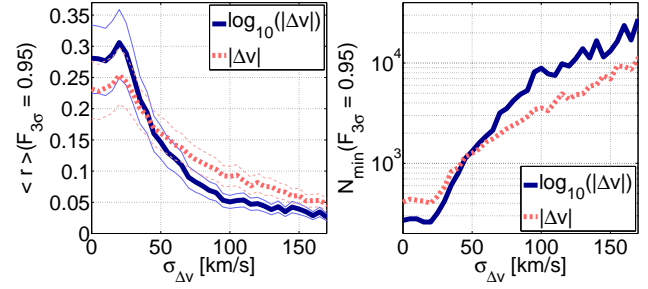


Figure 12. The figure shows the impact of random errors in the velocity offset; the error is assumed to be Gaussian with a standard deviation of $\sigma_{\Delta v}$. The right-hand panel shows the increase in the minimum number of QSOs (N_{min}) required to detect correlations between Σ_{dust} and $\log_{10}(|\Delta v|)$ (blue solid curves), or between Σ_{dust} and $|\Delta v|$ (red dashed curves) in a subset of QSOs with $\Sigma_{\text{dust}} > 0$ and $|\Delta v| \geq 45$ km/s, as $\sigma_{\Delta v}$ increases. Curves in the left-hand panel, with $\pm 1\sigma$ errors, show the corresponding decrease in the correlation coefficient $\langle r \rangle$ (see text for more details). Note that measurement errors below $\sigma_{\Delta v} \leq 45$ km/s results with higher $\langle r \rangle$ and lower N_{min} values for the $\Sigma_{\text{dust}}-\log_{10}(|\Delta v|)$ correlation, while the $\Sigma_{\text{dust}}-|\Delta v|$ correlation appears to be stronger when $\sigma_{\Delta v} \geq 45$ km/s.

in $\Sigma_{\text{dust}} > 0$ with a standard deviation of σ_{Σ} . The results are similar to those shown in Fig. 12: we find that $\langle r \rangle$ decreases, and the minimum number of QSOs required to detect the correlation between Σ_{dust} and $\log_{10}(|\Delta v|)$ (N_{min}) increases with σ_{Σ} . For the case of $\sigma_{\Sigma} = 0.6$ g/m² $= 0.1 \times \Sigma_{\text{torus}}$, we find $\langle r \rangle = 0.27 \pm 0.05$, with a p -value of $p \approx 10^{-58}$, and $N_{\text{min}} = 290$. Thus, random Gaussian errors in $\Sigma_{\text{dust}} > 0$ have a very small effect on the $\Sigma_{\text{dust}}-\log_{10}(|\Delta v|)$ correlation.

Based on the above, we conclude that statistical errors on estimating the velocity offsets and obscuring column densities can diminish the correlations predicted in the idealized toy model. This is mostly due to the impact of these errors on the purity of selection of a sub-sample, intended to include only the most correlated QSOs. In the examples above, we find that this increases the number of QSOs required for a detection by an order of magnitude, but there is no indication that these errors will prevent a detection of the correlations in a large sample (tens of thousands) of QSOs.

Finally, as the distribution of SMBH masses in QSOs observable in different survey projects may vary significantly, we have considered how using higher SMBH masses (see Greene & Ho 2007, 2009 and Shen & Kelly 2012) affect our results. In these tests, we have also taken into account the possibility of a correlation between the SMBH mass and the mass of the stellar core (Ferrarese et al. 2006; Graham et al. 2011; Kormendy & Ho 2013). We have found that the increased SMBH masses lead fewer SMBHs escaping the galactic nucleus (an effect that should increase the number of SMBHs in the population showing $\Sigma_{\text{dust}}-|\Delta v|$ correlation), however they also lead to significantly smaller torus sizes, resulting with a net decrease in the correlation coefficient of a factor of ~ 2 . This demonstrates that although the strength of the $\Sigma_{\text{dust}}-|\Delta v|$ is sensitive to the underlying assumptions of the applied models, the $\Sigma_{\text{dust}}-|\Delta v|$ correlation itself is a robust result.

6 CONCLUSIONS

A large fraction of luminous QSOs are believed to be triggered by merger events, and if QSO activity often follows the coalescence of SMBHs in the merging nuclei, then a large fraction of all QSOs may have experienced recent gravitational recoil. While a handful of QSOs with large spatial or velocity offsets have been identified as recoil candidates (Komossa 2012), the ubiquity of this phenomenon remains poorly known.

Here, we proposed a statistical technique to search for a population of recoiling SMBHs with smaller velocity offsets among luminous QSOs, based on a positive correlation between these velocity offsets and the column densities of obscuring dust tori. The correlations are introduced by the damped oscillating motions of SMBHs with typical recoil speeds, which are comparable to the escape velocities from galactic nuclei. These SMBHs spend a significant time off-nucleus, and at distances comparable to the size of obscuring tori in located in the nuclei.

We have demonstrated, using simple models of gravitational recoil, SMBH trajectories, and the geometry of obscuring dust tori, that observing a random sample of a few thousand partially obscured QSOs, with line-of-sight velocity offsets $|\Delta v| \geq 45$ km/s, could allow a significant detection of the correlation between the line of sight dust column density Σ_{dust} and $|\Delta v|$ (or $\log_{10}(|\Delta v|)$).

The existence of this correlation is found to be robust within the simple models we choose, and detectable even in the face of random errors on Σ_{dust} and $|\Delta v|$. However, we expect that the tightness of the correlation, the underlying $\Sigma_{\text{dust}} - |\Delta v|$ relation, and the properties of the QSO subset showing correlations can depend strongly on the model assumptions. Nevertheless, our results should motivate searching for correlations in real data; a positive detection would allow testing various combinations of recoil, BH trajectory, and dust tori models. A further test could be possible by comparing the predicted fraction of obscured QSOs to the observed fraction of type II QSOs. We propose to carry out these tests in the future using catalogues of observational data for QSOs, such as the SDSS-DR10 QSO catalogue.

ACKNOWLEDGEMENTS

The authors would like to thank Bence Bécsy, Gergely Dály, and Ákos Szölgyén for useful discussions and for valuable comments on the manuscript. Péter Raffai is grateful for the support of the Hungarian Academy of Sciences through the 'Bolyai János' Research Scholarship programme. We also acknowledge financial support from the NASA Astrophysics Theory Program under grant no. NNX11AE05G (to ZH) and from OTKA under grant no. 101666 (to ZF).

REFERENCES

Aller M. C., & Richstone D., 2002, *AJ*, 124, 3035
 Antonucci R., 1993, *Ann. Rev. A. & A.*, 31 473
 Baker J. G. et al., 2008, *ApJ*, 682, L29
 Barth A. J., Greene J. E., & Ho L. C., 2005, *ApJ*, 619, L151

Begelman M. C., Blandford R. D., & Rees M. J., 1980, *Nature*, 287, 307
 Blecha L. et al., 2011, *MNRAS*, 412, 2154
 Blecha L. et al., 2015, preprint (arXiv:1508.01524)
 Bogdanović T., Reynolds C. S., & Miller M. C., 2007, *ApJ*, 661, L147
 Bonning E. W., Shields G. A., & Salviander S., 2007, *ApJ*, 666, L13
 Comerford J. M. et al., 2009, *ApJ*, 698, 956
 Dubois Y. et al., 2014, *MNRAS*, 440, 2333
 Ferrarese L. et al., 2006, *ApJ*, 644, L21
 Georgiev I. Y., & Böker T., 2014, *MNRAS*, 441, 3570
 Gerosa D. et al., 2015, *MNRAS*, 451, 3941
 Graham A. W. et al., 2011, *MNRAS*, 412, 2211
 Greene J. E., & Ho L. C., 2006, *ApJ*, 641, L21
 Greene J. E., & Ho L. C., 2007, *ApJ*, 667, 131
 Greene J. E., & Ho L. C., 2009, *ApJ*, 704, 1743
 Gualandris A., & Merritt D., 2008, *ApJ*, 678, 780
 Guedes J. et al., 2009, *ApJ*, 702, 890
 Guedes J. et al., 2011, *ApJ*, 729, 125
 Haehnelt M. G., 1994, *MNRAS*, 269, 199
 Healy J., Lousto C. O., & Zlochower Y., 2014, *Phys. Rev. D*, 90, 104004
 Hönig S. F., 2008, Dr. rer. nat. dissertation, Rheinische Friedrich-Wilhelms-Universität
 Ivanov P. B., Papaloizou J. C. B., & Polnarev A. G., 1999, *MNRAS*, 307, 79
 Ju W. et al., 2013, *ApJ*, 777, 44
 Komossa S., 2012, *Adv. Astron.*, 2012, 364973
 Komossa S., & Merritt, D., 2008, *ApJ*, 689, L89
 Kormendy J., & Ho L. C., 2013, *ARA&A*, 51, 511
 Ledoux C. et al., 2015, *A&A*, 580, A8
 Leigh N., Böker T., & Knigge C., 2012, *MNRAS*, 424, 2130
 Loeb A., 2007, *Phys. Rev. Lett.*, 99, 041103
 Lousto C. O. et al., 2012, *Phys. Rev. D*, 85, 084015
 Madau P., & Quataert E., 2004, *ApJ*, 606, L17
 Martini P., 2004, in Ho L. C., ed., *Coevolution of Black Holes and Galaxies*, Cambridge Univ. Press, Cambridge, p. 170
 Pâris I. et al., 2014, *A&A*, 563, A54
 Reynolds C. S., 2013, *Class. Quantum Gravity*, 30, 244004
 Schartmann M. et al., 2005, *A&A*, 437, 861
 Sesana A., Haardt F., Madau P., & Volonteri M. 2005, *ApJ*, 623, 23
 Shen Y., & Kelly B. C., 2012, *ApJ*, 746, 169
 Shen Y., Liu X., Loeb A. & Tremaine S., 2013, *ApJ*, 775, 49
 Tanaka T. & Haiman Z., 2009, *ApJ*, 696, 1798
 Tremaine S. et al., 2002, *ApJ*, 574, 740
 Volonteri M., Haardt F., & Madau P., 2003, *ApJ*, 582, 559